Processing of interlaced images in 4–10 MeV dual energy customs system for material recognition

S. Ogorodnikov and V. Petrunin

Efremov Scientific Research Institute, St.-Petersburg, Russia

(Received 2 October 2000; revised manuscript received 13 November 2001; published 8 October 2002)

The aim of this article is to demonstrate the practical value of radioscopic differentiation of materials in the 1–10 MeV energy range to the work of customs services. The proposed method for achieving singling out and identifying four basic groups of materials according to an atomic number is complex. Atomic numbers are identified using high- and low-energy profiles obtained through the irradiation of materials on an alternate pulse-by-pulse basis. This is done using a bremsstrahlung beam with 8 MeV/4 MeV dual boundary energies and by using scintillating crystals coupled with silicon photodiodes as detecting elements. An image segmentation technique is then used to discern the distribution of an atomic number on any given image. The color visualization of integral absorption and a material's atomic composition is carried out according to the intensity hue saturation (IHS) colorization scheme. The experiments were carried out on a full-scale prototype of an 8 MeV customs inspection system developed by the Efremov Research Institute.

DOI: 10.1103/PhysRevSTAB.5.104701 PACS numbers: 87.59.Hp

I. INTRODUCTION

The well-known dual energy method of material discrimination is widely used in x-ray inspection systems for scanning hand luggage for customs and other security purposes [1–8]. Its major advantage over single-energy systems is its ability to differentiate between materials according to their atomic number. Such inspections allow customs officials to determine the presence of contraband in inspected cargo in two ways: as far as integral absorption is concerned and as far as atomic numbers are concerned. (The distribution of the latter is displayed on the official's workstation screen).

The differentiation of materials is achieved by comparing the attenuation ratio of low-energy x rays to high-energy x rays. Discrimination is possible because different materials have different degrees of attenuation for high- and low-energy x rays and that allows one to identify "organic" (low Z) and "inorganic" (high Z) materials in the controlled object.

The typical boundary x-ray energies for such installations do not exceed 200 kV due to the strong dependence of a total absorption coefficient from the atomic number due to the prevailing of photoelectric interaction ($\sigma_\tau \sim Z^5$) in this energy range.

Unfortunately, the penetrability of low-energy x rays is limited to a few centimeters of steel. That makes it useless for the inspection of shipping containers and vehicles. For such applications only high-energy x rays with a boundary energy of up to 10 MeV can be used, providing high quality radioscopic imaging of an inspected object.

However, the x-ray dual energy technique can still be used for the discrimination of materials in a high-energy range, but to date this has not been demonstrated in practice. This is possible because the method encounters physical obstacles in so far as 1–10 MeV is in the range of domination of the Compton effect with its poor Z dependence $\mu_c \sim Z/A$ (Figs. 1 and 2). This ratio is approximately the same for elements from, at least, the top of the periodic table, and the composition of those defines the whole variety of organic substances. The slight absorption variation between materials in the megavolt range occurs due to the pair production effect $\mu_\kappa \sim Z^2/A \sim Z$, but was previously considered to be insufficient for discriminatory purposes and almost useless for practical applications [9]. Single energy systems can only be used therefore for the inspection of vehicles and containers.

Recently a few ideas were elaborated to bypass the aforementioned physical limitations and to obtain the desired discrimination in a high-energy range. The first of these [10] involves the decomposition of transmitted x-ray spectrum onto the components responsible for the Compton effect and pair production, the balance of which

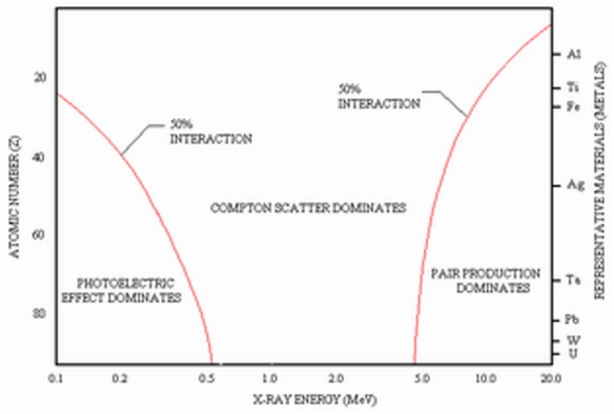

FIG. 1. (Color) Dominant gamma attenuation process for elements (atomic number Z) in gamma energy range 0.1 to 20 MeV.

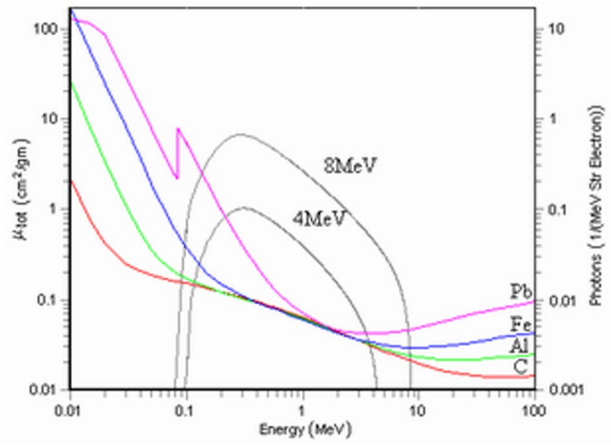

FIG. 2. (Color) Total attenuation coefficient as a function of energy for four elements. Grey curves are spectral distributions of bremsstrahlung quanta from a thick tungsten target of 8 and 4 MeV energies of an electron beam.

in transmitted spectrum determines the Z content of an irradiated barrier. The decomposition is due to the anisotropy of Compton scattering and the isotropy of pair annihilation gamma quanta, when x rays interact with high-Z material of a special detector target. However, the total sensitivity of this method seriously suffers from the substantial lowering of informative detector signals due to the scattering of transmitted x rays on the target.

The second type of proposed discrimination in a high-energy x-ray range uses a spectral filtering effect of bremsstrahlung [11,12]. During the scanning there are two different attenuation profiles corresponding to two different energy spectra: one without a filter and one with a filter. The atomic number of the material is evaluated from a special reference table, which is created by a calibration procedure. In two alternative embodiments either the electron beam is deflected onto two different targets or two bremsstrahlung filters are mechanically oscillated between the pulses of the accelerator. The major disadvantage of this method is its low sensitivity due to the low degree of spectrum hardening by any existing materials. This method suffers therefore from a low signal-to-noise ratio and can barely be realized with satisfactory image quality.

The aim of this article and our recent publications [13–15] is to demonstrate the practical value of radioscopic differentiation of materials in the 1–10 MeV energy range to the work of customs services. The proposed method for achieving singling out and identifying four basic groups of materials according to atomic number is complex. Atomic numbers are identified using high- and low-energy profiles obtained through the irradiation of materials on an alternate pulse-by-pulse basis. This is done using a bremsstrahlung beam with 8 MeV/4 MeV dual boundary energies and by using scintillating crystals coupled with silicon photodiodes as detecting elements. An image segmentation technique is then used to discern the distribution of an atomic number on any given image. The color visualization of integral absorption and a material's atomic composition is carried out according to the IHS scheme. The experiments were carried out on a full-scale prototype of an 8 MeV customs inspection system developed by the Efremov Research Institute.

II. PHYSICAL BACKGROUND

It is known that a certain noise level is always inherent to practical measurements, therefore, let us numerically evaluate the discrimination effect and compare it with the accuracy of experimental measurements in order to estimate whether the distinction between materials is possible at all.

The radioscopic transparency of material with a mass thickness t and an atomic number Z for a bremsstrahlung beam with boundary energy E_e is expressed as a ratio of radiation intensity before and after the penetration of a barrier:

$$T(E_e, t, Z) = \frac{\int_0^{Ee} \frac{dP}{dE_\gamma}(E_e, E_\gamma) e^{-\mu(E\gamma, Z)t} dE_\gamma}{\int_0^{Ee} \frac{dP}{dE_\gamma}(E_e, E_\gamma) dE_\gamma}, \quad (1)$$

where the integrand function is a product of bremsstrahlung intensity according to the Schiff formula [16] and the detector response factor [17]:

$$\frac{dP}{dE_\gamma}(E_e, E_\gamma) = \frac{dI}{dE_\gamma}(E_e, E_\gamma)(1 - e^{-\mu_{\text{det}}(E\gamma)t_{\text{det}}}) \frac{\mu_{\text{det}}^{en}(E_\gamma)}{\mu_{\text{det}}(E_\gamma)}. \quad (2)$$

During the irradiation of the barrier with nominal and dual boundary energies, two transparency profiles are obtained, and the evaluation of the atomic number and the mass thickness of a material can be formulated as a solution of a system of integral equations [13]. In general the solution cannot be found in so far as the barrier can represent a heterogeneous mixture of materials and, therefore, a number of unknown variables might exceed the number of equations. Nevertheless, even in such cases the atomic number still can be evaluated as a weighted mean of barrier's constituent components.

In order to ascertain the possibility of discrimination according to Z and to estimate the effect, it is useful to introduce a ratio of logarithmic transparencies (inverse value of absorption) at the nominal E_1 and dual E_2 boundary energies of bremsstrahlung:

$$R(E_1, E_2, t, Z) = \frac{\ln T(E_1, t, Z)}{\ln T(E_2, t, Z)} = \frac{\overline{\mu}_{\text{eff}}(E_1, t, Z)}{\overline{\mu}_{\text{eff}}(E_2, t, Z)}. \quad (3)$$

It is evident that for the monochrome gamma beam the ratio (3) is simply the ratio of the total absorption coefficients at the nominal and dual energies, which is a constant and uniquely characterizes irradiated material.

For cases with broad bremsstrahlung spectrum with dual boundary energies, which we are looking at, the aforementioned ratio becomes sensitive to the mass thickness of the material. This phenomenon is achieved by the hardening of the x-ray spectrum during its penetration through a barrier. Ratio (3) can be treated as a ratio of effective absorption coefficients, averaged over a bremsstrahlung spectrum.

The ratio represents a monotonic function of an atomic number at $E_1 = 8$ MeV and $E_2 = 4$ MeV for most of the mass thickness range, except the region of thin barriers (Fig. 3). Because of this fact atomic numbers can be simply approximated for a given value of the ratio (3) and attenuation rate at one of the energies, so a lookup table can be created for the direct calculation of Z from experimentally measured high- and low-energy transparencies.

This scenario is not so good for a region with small mass thickness, where the contribution of the photoeffect into the absorption rate of elements with a high atomic number is significant and gives rise to discrimination ambiguity. For example, the ratio is approximately the same for carbon and lead for barriers with 10 gm/cm^2 mass thickness and, therefore, these materials cannot be distinguished.

Nevertheless, the ambiguity of discrimination can be minimized or completely removed by the preliminary filtering of the soft part of the bremsstrahlung spectrum.

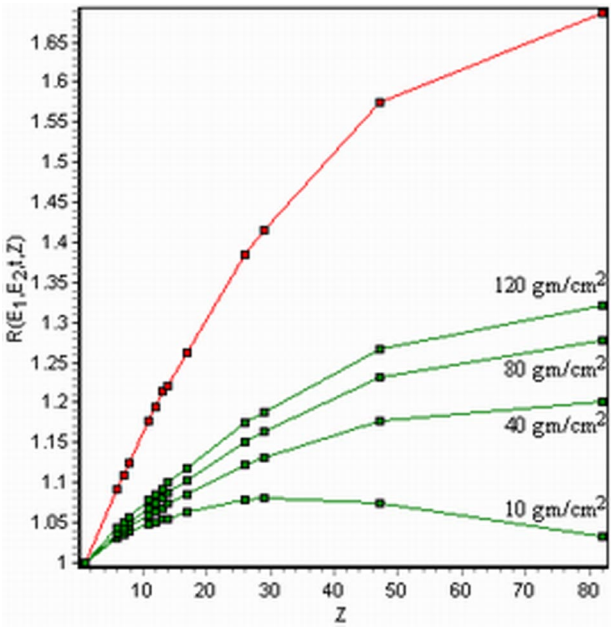

FIG. 3. (Color) Ratio $R(E_1, E_2, t, Z)$ vs atomic number Z for barriers with different mass thickness (green curves). Values correspond to the following materials: H, C, N, O, Na, Mg, Al, Si, Cl, Fe, Cu, Ag, and Pb. A red curve illustrates monochromatic 8/4 MeV gamma beams. Ratio is normed to hydrogen. Analytical calculation for pencil beams geometry.

The best candidate for such a filter is a material with a high atomic number such as lead. The proper choice of filter thickness is a tradeoff between the degree of ambiguity for thin barriers and signal-to-noise ratio deterioration.

Figure 4 demonstrates that radioscopic discrimination is possible irrespective of the thickness of the material. One can observe the separation of absorption curves for some elements from the periodic table given as the ratio (3) versus mass thickness.

The discrimination effect between a pair of materials with atomic numbers Z_1 and Z_2 can be numerically evaluated according to the following expression:

$$D(Z_1, Z_2, t) = \left(1 - \frac{R(t, Z_2)}{R(t, Z_1)}\right)100\%. \qquad (4)$$

From a practical point of view, it is worthwhile evaluating the discrimination effect (4) not only for the ideal case of the pencil beam with exponential attenuation (1) but also for a fan-shaped x-ray beam used in radioscopy. In the fan-shaped beam the flow of transmitted quanta is affected by the fluence of scattered ones, appearing due to the Compton effect, which is dominant in our energy range.

The Monte Carlo simulations were performed for the polyethylene ($Z \approx 5.3$, $\rho = 1.1$ gm/cm^3), water ($Z \approx 7.2$, $\rho = 1.0$ gm/cm^3), aluminium ($Z = 13$, $\rho = 2.7$ gm/cm^3), iron ($Z = 26$, $\rho = 7.89$ gm/cm^3), and lead ($Z = 82$, $\rho = 11.3$ gm/cm^3) barriers with equal mass thicknesses 10, 40, 80, and 120 gm/cm^2 at 8 and 4 MeV boundary energies of radiation beam.

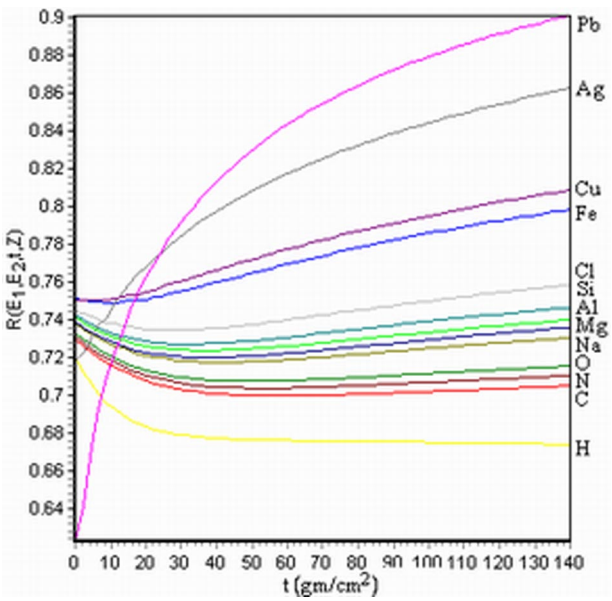

FIG. 4. (Color) Ratio $R(E_1, E_2, t, Z)$ vs mass thickness t at 8/4 MeV for different elements. Analytical calculation for pencil beams geometry.

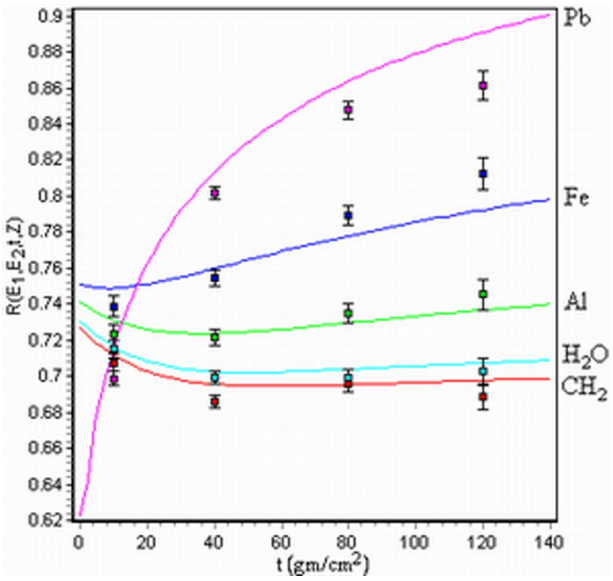

FIG. 5. (Color) Results of Monte Carlo simulations of discrimination effect at 8/4 MeV for polyethylene, water, aluminium, iron, and lead for barriers 10, 40, 80, and 120 gm/cm^2 in fanlike beam geometry (shown as rectangles). Curves are given for the pencil beams geometry.

A digital model of the numerical experiment assumed the flow of initial bremsstrahlung quanta in a fan-shaped form. The detector line was aligned with a beam and represented as a set of $CdWO_4$ $3 \times 3 \times 20$ mm crystals. Tested materials were shaped as barriers with a preset mass thickness in the direction of beam propagation and limitless thickness in two other directions. Cross section data for the tested materials were taken from [17]. Digitally modeled detectors measured the transparency of a barrier (1).

As it is seen (Fig. 5) for the practically interesting mass thickness range, the results are closely related to the ones obtained for the pencil beam.

We see that the effect is negligible for the materials with similar atomic numbers. For example, for water and polyethylene with $\Delta Z \approx 2$ it totals only about 1%, but between polyethylene and iron $\Delta Z \approx 20$ it is already around 10%. Discrimination slightly increases with thickness growth as far as x-ray spectrum undergoes hardening and approaches the monochrome one (Fig. 3).

Thus, from the above consideration one can see that dual energy radioscopic material discrimination according to Z is possible, but its practical realization requires accurate measurements of transparencies (with the precision of at least three significant digits).

III. EXPERIMENTS

In order to ascertain how significant the value of the discrimination effect between different materials really is, it is reasonable to perform experiments using conventional customs inspection equipment.

For this purpose a series of experiments was carried out on a full-scale prototype of a customs inspection system developed and manufactured by the Efremov Research Institute [15]. The basic technological equipment of the system included the following units.

(i) Industrial linear electron accelerator with energy 8 MeV at the nominal mode and 4 MeV at dual one. Pulse duration: 5 μ sec; repetition rate: 100 Hz.

(ii) Collimating system forming a 4 mm vertical fan-shaped bremsstrahlung beam consisting of the primary and secondary collimators and a scatter-suppressing collimator in front of the detector line (Fig. 6).

(iii) Detector line with $CdWO_4$ crystals coupled with PIN diodes as sensitive elements with 3.5 mm pitch.

(iv) Transportation system of tested objects.

During the experiment an inspected object was moved by the transportation system across the fan-shaped bremsstrahlung beam formed by the collimation system. The sensitive elements of the detector line registered bremsstrahlung quanta penetrated through the object. The signal from the detectors was digitized, initially processed, and transferred to a workstation, where a radioscopic image was formed.

FIG. 6. (Color) Collimation system forming a 4 mm fan-shaped beam.

The accelerator operated in a so-called interlaced mode, when each even pulse generated a high-energy bremsstrahlung and each odd pulse a low one. Such a scheme allowed the forming of dual radioscopic images containing two transparency profiles with different energies.

The scanning scheme assumed to be used in the customs inspection with 40 cm/sec scan speed implies that the accelerator emits pulses with high and low energy by couples with a preset repetition rate. Small temporal shifts between pulses allow the reduction of a spatial shift between images with high and low energy.

In order to simulate such a scanning scheme in our experiments the speed of the container was deliberately lowered and the detector line registered only a couple of neighboring high-low-energy pulses skipping a subsequent series of pulses until it registered the next couple. Thus, during the experiment each image column (for high and low energy) was formed by the acquisition of only a single couple of accelerator pulses.

Though the real speed of the container in our experiments was slow enough, such a scheme allowed us to simulate a real system, where the modulator of an accelerator generates pulses by couples with a normal repetition rate (100 couples/sec).

Preliminary processing steps of the raw dual data included the following.

(i) Decomposition of interlaced data into the high- and low-energy profiles.

(ii) Correction of temporal dose rate fluctuations of accelerator for both profiles.

(iii) Correction of the angular anisotropy of bremsstrahlung intensity as well as the nonuniformity of detectors including gain, offset, and nonlinearity.

(iv) Evaluation of bremsstrahlung boundary energy of both profiles by the absorption method [18] for the creation of the atomic number lookup table.

As a tested object for transparency evaluation, a steel step wedge with 2.5, 5.0, 7.5, 10.0, and 15.0 cm steps was taken. The primary bremsstrahlung was filtered through a 0.4 cm lead plate. In the experiment, the boundary energies of high and low x-ray beams evaluated by the absorption method equaled 7.5 and 4.6 MeV correspondingly. The radiation dose absorbed by detectors per pulse (image column) totaled 330 μGy for the high energy and 30 μGy for the low one. Both transparencies were obtained by averaging pixels belonged to each barrier and given in Table I. The spread of ratio (3) for each step is demonstrated in Fig. 7. It is necessary to note that preliminary filtering of bremsstrahlung spectrum by lead allowed us to translocate the crossing point of Fe and Pb curves from 20 gm/cm^2 (Fig. 4) to 10 gm/cm^2 and, therefore made it possible to extend the mass thickness range of unambiguous recognition of four material groups.

In order to analyze the measured values, it is worthwhile assessing how effective the discrimination is.

Suppose we have only two groups of materials: organic, adequately characterized by hydrocarbon ($Z_1 \approx 5.3$), and inorganic, represented by iron ($Z_2 = 26$). Then the probability of making a decision that a data point belongs to one of two groups can be written in accordance with the Bayesian formula (5) and numerically estimated for different attenuation rates [19].

$$P(w_j|R) = p(R|w_j)P(w_j)/p(R), \tag{5}$$

where $P(w_j|R)$ is *a posteriori* probability of tested material w_j being *organic* or *inorganic* for a data point R. For simplicity's sake let us make equal the prior probabilities of both groups and conditional densities which $p(R|w_j)$ are normally distributed with the mean variance given in Table I. The average error probability rate over all possible measurements can be calculated using the Bayesian law of total probabilities, which implies that

$$P_{\text{err}} = \int_{\text{all}R} p(R) \min_{w_j}[p(w_j|R)]. \tag{6}$$

TABLE I. Experimentally measured transparency T and signal-to-noise ratio SNR as a function of mass thickness for high E_1 and low E_2 energy images. Data are given for a steel step wedge. Ratio R and its error δ_R, discrimination effect for hydrocarbon and steel $D_{CH2,\text{Fe}}$ and their discrimination error P_{err} are given also.

	Mass thickness t, gm/cm^2					
	0	20	40	60	80	120
$T(E_1)$	1.0	0.4368	0.2039	0.0989	0.0491	0.0127
SNR_1	221	136	98	64	42	23
$T(E_2)$	1.0	0.3732	0.1527	0.0658	0.0295	0.0065
SNR_2	76	43	27	17	9	4
R	...	0.843	0.847	0.851	0.856	0.864
δ_R	...	2.4%	2.1%	2.3%	3.3%	5.2%
$D_{CH2,\text{Fe}}$	...	5.9%	7.0%	7.8%	8.4%	9.4%
P_{err}	...	9.9%	3.4%	4.5%	10.8%	19.7%

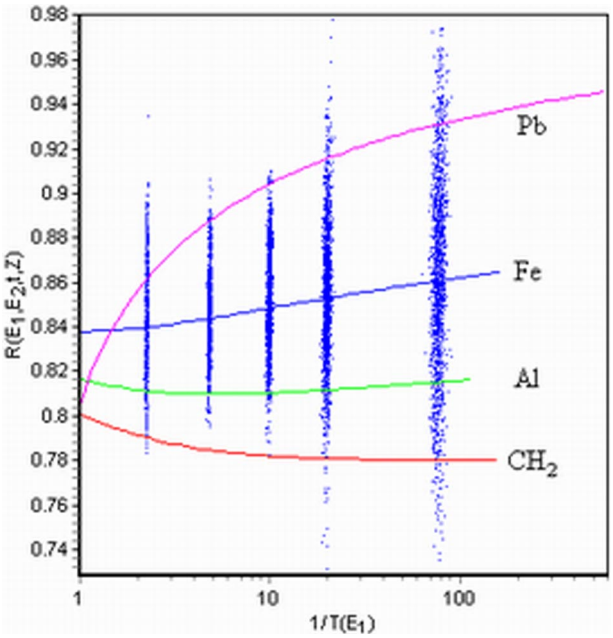

FIG. 7. (Color) Spread of experimentally measured ratio $R(E_1, E_2, t, Z)$ at nominal $E_1 = 7.5$ MeV and dual $E_2 = 4.6$ MeV for 2.5, 5.0, 7.5, 10.0, and 15.0 cm steel barriers plotted versus absorption rate at nominal energy. In this experiment a 4 mm lead filter of bremsstrahlung spectrum was used. Absorption curves of materials are given for mass thickness up to 140 gm/cm^2.

The estimates show, for example, an error rate for a barrier with 40 gm/cm^2 mass thickness equals 3.4%. That means for the given variance of dual data the probability to recognize a 5 cm steel barrier as an inorganic substance equals 96.6% and, correspondingly, as an organic one, 3.4%.

The 40–60 gm/cm^2 mass thickness range is optimal for material recognition and characterized by minimal discrimination error. However, the thinner barriers do deliver better signal-to-noise ratios for both transparencies although they do not provide sufficient contrast between them. On the other hand, the thicker barriers do not let enough numbers of low-energy quanta to penetrate through. The result sits well with estimates of the optimal uncertainty in transmission experiments given in [20].

Thus, the radioscopic material discrimination in our energy range is realizable for almost the entire mass thickness range. In the simplest case, when only organic-inorganic separation is needed, the satisfactory solution is achievable for the optimal mass thickness range even without any processing of dual data.

Nonetheless an attempt to perform discrimination of materials belonging to other groups or the same group faces problems as experimental data spread might exceed the discrimination effect itself. For example, discrimination between hydrocarbon and aluminium ($Z = 13$) for a 40 gm/cm^2 barrier leads to 21% error. Replacement of aluminium with water ($Z \approx 7.2$) raises the error rate to 42%.

FIG. 8. (Color) Photograph of shipping container with cargo and hidden contraband.

Thus, in the more common case, for example, of four groups of materials, being scanned for customs purposes, the effectiveness of discrimination is reduced and material recognition becomes unreliable. This is demonstrated on a colored fragment of a shipping container (Fig. 8), where material recognition is fulfilled on the pixel-by-pixel basis for four groups of materials without any processing of data (Fig. 9). The color scheme used is carried out according to the IHS scheme [21], and is the most suitable for visualization of the integral absorption and Z content of the materials. In the IHS scheme used for our task, intensity denotes transparency, color represents atomic number, and saturation characterizes the degree of material discrimination. The visualization of four material groups with the color encoding according to Table II was used.

One can see from this that the image is heavily corrupted by incorrectly recognized pixels, which appear as random color freckles. This effect does not allow us to distinguish small details such as the contour of a revolver, which would hardly be recognized against a background of sacks filled with sawdust.

However, this drawback can be overcome. Namely, by using denoising methods based on perception features of human vision, which extracts separate segments only, and applying these to a dual image. Such methods—known as image segmentation techniques—are widely used in pattern recognition and image analysis and [22] will be discussed in the following section.

IV. SEGMENTATION TECHNIQUE

As we have seen the pixel-by-pixel treatment of images does not produce satisfactory results because pixels are processed independently and only their transparencies

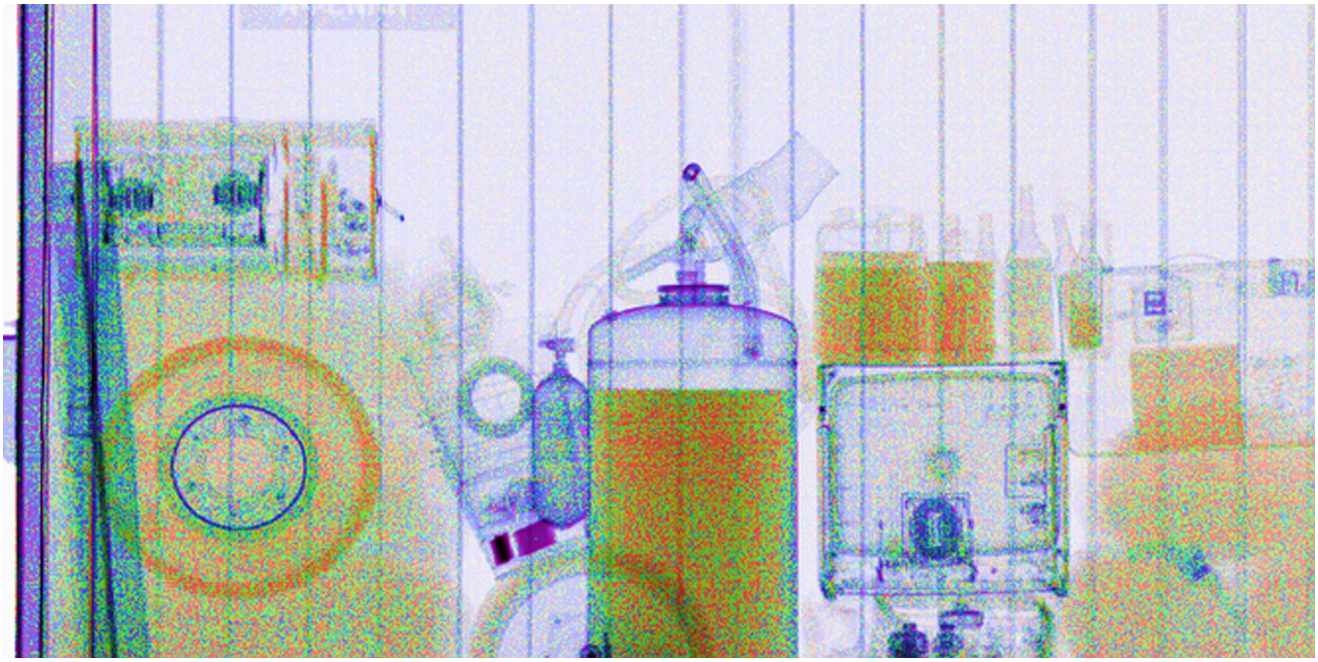

FIG. 9. (Color) An image of a shipping container with the assignment of colors according to Table II. Colorization of dual data is fulfilled on pixel-by-pixel basis without any processing. Left to right: oscillograph on sacks filled with sawdust, wheel, rifle cartridges hidden in the inner tube of the wheel, two lead bars, large fire extinguisher, liquid filled bottles on a TV set, case with plastic inside, a revolver below, hidden in sacks filled with sawdust.

are taken into account. This neglects the implicit spatial information that is available in the image.

Usually, a shipping container or a truck filled with a heterogeneous medium constituted the different type of cargo. Such an object being exposed to x rays forms a radioscopic image that is composed of thousands of distinct homogeneous segments, which can be easily distinguished and perceived as whole by the human visual system. It is evident that material recognition must be fulfilled for whole segments also on the basis of both spectral and spatial information, taking into account the pixel's belonging to a given segment. For example, a bottle with liquid or a bar of gold can be treated as two different objects with the assignment of different individual labels to the corresponding pixels. Subsequent association of the labels with color gives us the possibility to form a segmented image.

In general, spatial information can be taken into account by the averaging of a pixel's neighborhood according to the known linear and nonlinear schemes [23–25]. However, in our task the adequate smoothing demands a crucial enlargement of the size of a moving window (at least up to a typical size of a segment on the image). This raises the time consumption of processing to the extent that it makes the method useless for the practical applications.

TABLE II. Benchmarks for material-to-color conversion.

Media	Material	Z	Hue
Organics	Hydrocarbon	5.3	Orange
Organics-inorganics	Aluminum	13	Green
Inorganics	Iron	26	Blue
Heavy substances	Lead	82	Lilac

The problem we have touched on is closely related to another, known in the dual-echo magnetic resonance tomography [26] and also to multispectral [27] and color [28] image segmentation. In such treatment schemes the processed image is divided into a fixed number of meaningful regions and each of them is characterized by a set of unique properties (for example, intensity and color).

A similar segmentation technique can be applied to the processing of two dual radioscopic images, using the following three steps.

(i) The first step is to perform a rough segmentation of an image according to a data clustering algorithm.

(ii) The second step reduces the oversegmentation by selectively merging neighboring regions with a small area.

(iii) And the third one labels the surviving clusters and associates them with cargo substances.

The quality of segmentation depends mainly on the choice of the clustering algorithm, which, in our case, is determined by a couple of limitations.

First, the result of clustering should not depend on the number of partitionings. The small number might lead to

the loss of small, but essential objects, the bigger one to undesired oversegmentation. The right choice of the given parameter requires some *a priori* knowledge about the image (the "ground truth"), but in the case of containers with arbitrary cargo we know nothing in advance.

Second, the high-resolution radioscopic images of long containers usually contain a few million pixels. In our task the image processing time must not exceed a few minutes due to the requirement of high throughput of the system. That forces us to use a noniterative scheme of clustering only.

The algorithm, which suits the above conditions is the Leader algorithm [29] or 1-pass k-means algorithm [30]. The Leader algorithm assigns each data point to a class based on one of the following: evaluation of distance between an input data point to an existing cluster and comparison of it with a "vigilance" distance for a decision if the data point belongs to the cluster or is a prototype (a "leader") for a new one. Though the Leader algorithm is conventionally treated as an approach, which achieves computational efficiency at the expense of precision [31], being applied to the dual energy radioscopic images, it produces surprisingly good results.

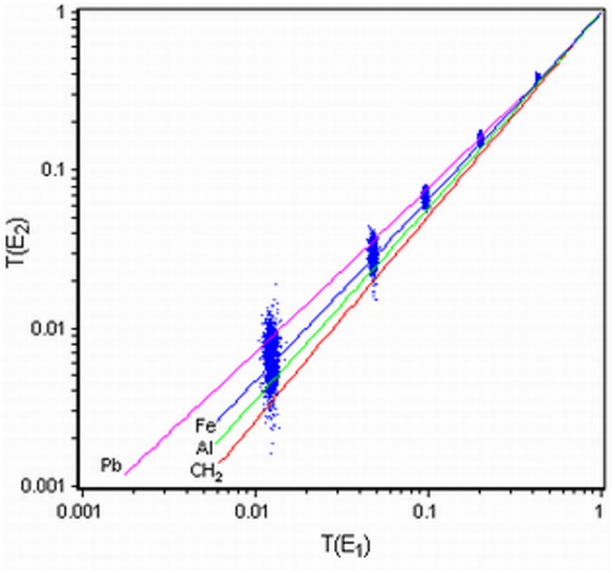

FIG. 10. (Color) Scatter plot of dual energy radioscopic data: bottom axis: high-energy (7.5 MeV), left: low-energy (4.5 MeV) transparency. Data are given for a steel step wedge with the thicknesses: 2.5, 5.0, 7.5, 10.0, and 15.0 cm. Curves of materials are given for mass thickness up to 140 gm/cm^2.

A. Leader clustering

For the reliable partition, it is necessary to assume that each step of the tested step wedge is treated as a separate image segment. The clusters, corresponding to 2.5, 5.0, 7.5, 10.0, and 15.0 cm steps of the steel step wedge, are shown on the scatter plot with axes given by high- and low-energy transparencies (Fig. 10). They represent ellipses, whose dimensions are a function of the spread of measured transparencies. The edge of the ellipse forms a decision boundary for the cluster. If a data point (pixel) drops within a decision boundary, a label of the corresponding cluster is assigned to the pixel.

It is natural to suppose that the length of ellipse axes has to be not less than 3 standard deviations for both transparencies. In such a case, for the Gaussian distribution 99.7% of pixels, belonging to a step of the step wedge, drop into a single cluster.

As we have seen, the measurements of transparencies are significantly affected by noise, which corrupts the image partitioning. This mainly concerns a low-energy image since in the experiments the intensity of the primary bremsstrahlung is approximately 10 times less than the same for the high one. That causes the overlapping of clusters with similar transparencies and even their merging together. This effect is seen in Fig. 10, where clusters of the steel step wedge overlap transparency curves for hydrocarbon, aluminium, and lead. Employment of statistical classification methods does not allow us to separate clusters of different materials with equal mass thickness.

Nevertheless, it is possible to separate the merging clusters, if their geometrical disposition is taken into account. Clusters, overlapping on the scatter plot but corresponding to spatially disjoined objects must be treated as different clusters in spite of their similar means. This approach requires a modification to the classical Leader algorithm in order to take into account the spatial aspect of image data. In the new scheme a pixel is included in a certain cluster only if it is geometrically adjacent to the image of any of the members constituting the cluster. Thus, each cluster consists of pixels not only having similar transparencies, but spatially adjacent to each other. Geometrically disjointed objects on the image along with approximately equal Z constitute clusters with different labels. This permits a more accurate evaluation of cluster centers and, consequently, their atomic numbers.

It is evident that the result of partitioning depends on the processing order of pixels and that is a disadvantage of the algorithm. Nevertheless, as has been tested on real images, the final partitioning result for the desired objects is insensitive to the sequence order.

B. Oversegmentation

There is another drawback of the Leader clustering algorithm known as oversegmentation. The gross segments corresponding to the cargo objects are speckled with lots of smaller spots with false labels. Such an effect becomes apparent on an output image where the labels

of clusters are substituted by corresponding colors. The false colors of the small segments result in pepper-and-salt noise and heavily corrupt the final image as far as the number of small clusters is much greater than the gross ones (Fig. 11). Oversegmentation can be partially reduced, for example, by bilateral filtration [25] applied to high- and low-energy images as a preprocessing step.

In order to preserve the fine structure of the output image, a proper merging of irrelevant clusters has to be carried out. This scheme assumes an iterative merging of neighboring regions with similar transparencies. The merging criterion is taken from the hypothesis assuming that population means are equal. For small area clusters ($n < 30$) a student's T-test is most suited [32].

The process starts with the sorting of a cluster according to the area. A cluster with the smallest area is merged with one of its geometrical neighbors. A candidate for merging is selected if the means and standard deviations of both clusters produce the smallest student's T-test value. The merging of the cluster reiterates with other neighbors until a new cluster with an area exceeding a preset threshold is achieved. A newly appeared cluster contains information about the merged ones, and its means are the area-weighted means of its parents. The process continues till there are no clusters with an area less than the threshold.

The threshold is a subjective partition parameter chosen by the visual evaluation of output image quality. From our experimental observations the optimal results are achieved with a threshold of about 10 pixels. The lesser values do not eliminate the undesirable false-color freckles and the greater ones result in a coarse-grained image. Physically the threshold can be treated as the user defined minimal size of an object for which the atomic number can be evaluated. For example, in our experiments, the 9-pixel threshold corresponds to approximately 1 cm^2 object on image.

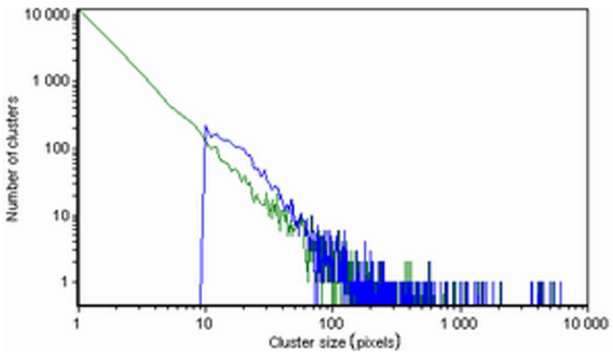

FIG. 11. (Color) Histogram of cluster size for 3s Leader partition (green) and after merging (blue). The threshold for merging is 9. Histogram is built for a 480×360 container image fragment (Fig. 12).

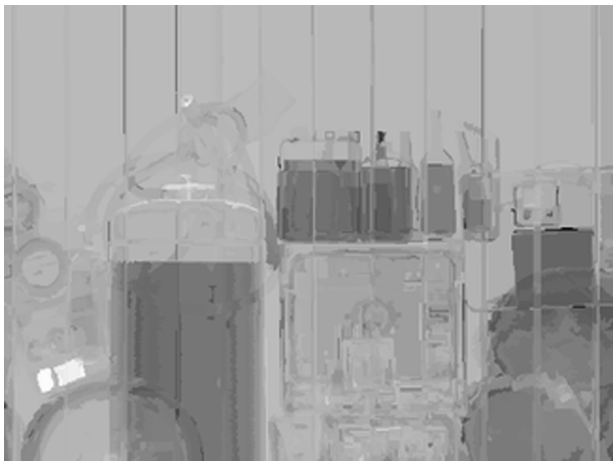

FIG. 12. Distribution of substances' atomic numbers on the fragment of a cargo container after segmentation.

As we have seen the threshold has to be preset differently relative to the geometrical size of detector crystals. In a certain sense this resembles the idea of utilizing larger crystals for the detection of filtered bremsstrahlung with low intensity for forming of a dual image [12]. In our case of the digital enlargement of the colored spots by cluster merging, the spatial resolution remains almost intact, as the spatial shape of the spots is effectively adapted to the variation of intensity on the image.

C. Labeling

Upon completion of the oversegmentation elimination, we obtain the partition of an image into a set of segments, whose cluster centers correspond to high and low transparency of singled out objects. If a pixel belongs to a certain cluster, then both its transparencies are replaced with ones of the cluster center, and the pixel is enumerated with the cluster label (number). The subsequent conversion of transparency into an atomic number is performed according to the predefined lookup table. The distribution of an atomic number on the image in a grey color after segmentation is demonstrated in Fig. 12.

Accordingly, the color representation of the same fragment is shown in Fig. 13. In comparison to Fig. 9, lots of new important details are revealed, for example, a revolver on the bottom right of the image.

V. CONCLUSION

The results of this paper can be summarized as follows.

Routine measurements of a dual integral absorption rate by the scintillator-photodiode pair in 1–10 MeV range

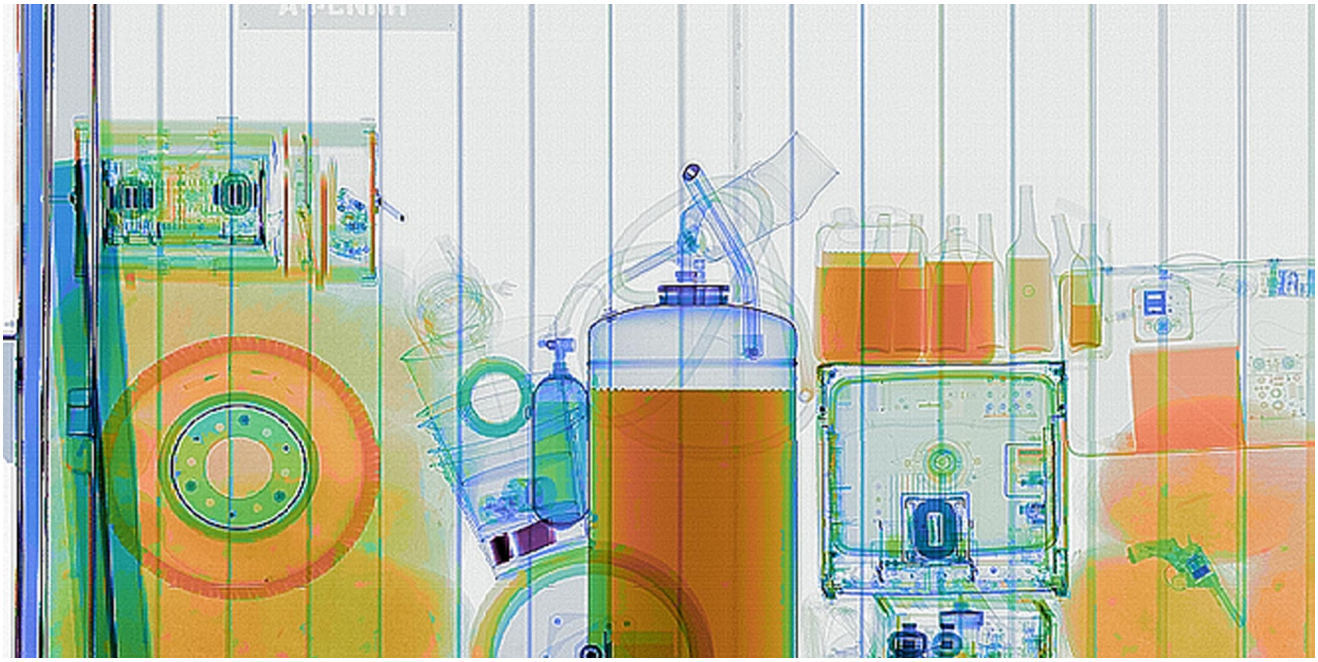

FIG. 13. (Color) Colorized image of a shipping container with color assignment according to Table II. Colorization is fulfilled after the segmentation procedure.

do not allow us to achieve the complete discrimination of materials in cargo containers.

The image segmentation technique based on the modified Leader clustering algorithm allows us to suppress noise on the dual images to a certain extent and perform discrimination of four basic material groups.

The dual energy radioscopic discrimination of materials according to an atomic number was demonstrated on a full-scale prototype of a customs inspection system with 8/4 MeV dual boundary energies.

ACKNOWLEDGMENTS

We are deep in debt to Mr. Andrew Osborn, who has taken a hard labor of careful reading and linguistic correction of this paper.

[1] http://www.as-e.com
[2] http://instruments.perkinelmer.com/
[3] http://www.rapiscan.com
[4] http://www.saic.com
[5] http://www.heimannsystems.com
[6] http://www.invision-tech.com
[7] http://egginc.com
[8] http://www.vividusa.com/
[9] J. F. Moore, V. C. Ravi Chandran, and R. F. Reiter, *PortTechnology International*, 10th ed., Vol. 4, p. 113, http://www.porttechnology.org/journals/ed10/download/PT10-04_1.pdf
[10] W. W. Neale *et al.*, U.S. Patent No. 5,524,133 (1996).
[11] P. J. Bjorkholm, U.S. Patent No. 6,069,936 (2000).
[12] D. Perion *et al.*, International Patent No. WO 00/43760 (2000).
[13] V. L. Novikov, S. A. Ogorodnikov, and V. I. Petrunin, Problems of Atomic Science and Technology **4**, 93 (1999), ISSN 1562-6016.
[14] S. A. Ogorodnikov, V. I. Petrunin, and M. F. Vorogushin, in *Proceedings of the 7th European Particle Accelerator Conference, Vienna, 2000* (European Physical Society, Geneva, 2000), http://accelconf.web.cern.ch/AccelConf/e00/index.html
[15] S. A. Ogorodnikov, V. I. Petrunin, and M. F. Vorogushin, in *Proceedings of the XXth International Linac Conference, 2000* (SLAC, Stanford, 2000), http://www.slac.stanford.edu/econf/C000821/proceedings.html
[16] L. J. Schiff, Phys. Rev. **83**, 252 (1951).
[17] E. Storm and H. Israel,"Photon Cross Section from 0.001 to 100 MeV for Elements 1 through 100," Los Alamos Scientific Laboratory, New Mexico, 1967.
[18] J. R. Greening, Br. J. Radiol., **20**, 230, 1947.
[19] http://www.cs.mcgill.ca/~mcleish/644/main.html
[20] E. J. Burge, Nucl. Instrum. Methods **144**, 547 (1977).
[21] W. J. Carper, T. M. Lillesand, and R. W. Kiefer, Photogramm. Eng. Remote Sens. **56**, 459 (1990).
[22] M. Sonka, V. Hlavac, and R. Boyle, *Image Processing, Analysis, and Machine Vision* (Chapman and Hall, London, 1993), 2nd ed.
[23] R. Fisher, S. Perkins, A. Walker, and E. Wolfart, *Hypermedia Image Processing Reference* (Wiley, New York, 1996).
[24] S. M. Smith and J. M. Brady, Int. J. Comput. Vision, **23**, 45–78 (1997).

[25] C. Tomashi and R. Manduchi, in *Proceedings of the 1998 IEEE International Conference on Computer Vision* (New Delhi, Bombay, India, 1998).
[26] G. Gerig *et al.*, Image and Vision Computing **10**, No. 6, 349–360 (1991), IPMI special issue.
[27] M. Zerbst *et al.*, University of Dortmund Technical Report No. 28-00, 2000, http://www.statistik.uni-dortmund.de/sfb475/berichte/tr28-00.ps
[28] A. Koschan and W. Skarbek, Technical University of Berlin Technical Report No. 94-32, 1994, http://cv.cs.tu-berlin.de/koschan/coseg.ps.gz
[29] H. Späth, *Cluster-Analyse-Algorithmen zur Objektklassifizierung und Datenreduktion*, edited by R.Oldenbourg (Verlag GmbH, München, Wien, 1977).
[30] http://www.ece.neu.edu/groups/rpl/kmeans/
[31] F. Murtagh and A. Heck, *Multivariate Data Analysis*, Astrophysics and space science library (D. Reidel Publishing Company, Dordrecht, 1987).
[32] J. Sijbers *et al.*, Magn. Reson. Imaging **15**, 679–688 (1997).